International Conference "Water, Environment, Energy and Society" (WEES–2009)
New Delhi, 12–16 January 2009

Vegetation and Climate Variability by Fourier Analysis of Multispectral Satellite Images

Li Jia
Alterra, Wageningen University and Research (WUR) Centre
Wageningen, The NETHERLANDS
E-mail: Li.Jia@wur.nl

Massimo Menenti
Istituto per i Sistemi Agricoli e Forestali del Mediterraneo—ISAFoM via Patacca 85 80056
Ercolano (NA), ITALY
E-mail: m.menenti@isafom.cnr.it
and
Laboratoire des Sciences de l'Image, de l'Informatique et de la Télédétection (LSIIT), Université
L. Pasteur, Strasbourg, FRANCE
E-mail: Massimo.Menenti@ensps.u-strasbg.fr

ABSTRACT: Satellite observations of the terrestrial biosphere cover a period of time sufficiently extended to allow reliable climatologies to be determined. The latter is particularly relevant for studies of vegetation response to climate variability. This chapter reviews work done by the authors since the late 80-s on the use of time series analysis techniques to extract concise information from extended time series of large area multispectral satellite data. Two basic methods have been used: the Fast Fourier Transform, especially in the earlier studies, and Harmonic Analysis in more recent work. Since our first study we have been relying on the global radiometric data collected by AVHRR and later on MODIS. The studies reviewed in this chapter have been preformed in different continents. The main applications documented by published results are: (a) identification and mapping of zones characterized by a similar response of terrestrial vegetation to environmental forcing; (b) determination and characterization of the response of terrestrial vegetation to climate variability over any period of time covered by available time series of satellite data; (c) early warning on anomalies in vegetation development of terrestrial vegetation using indicators of photosynthetic activity such as NDVI and fAPAR. These applications span a range of temporal and spatial scales, consistently with the nature of processes observed. We have shown, using data at low spatial and temporal resolutions, that at continental scale spatial patterns in vegetation types and their average pehenology are determined by climate, in particular dryness. The response of vegetation phenology to interannual climate variability required observations at significantly higher spatial and temporal resolutions. Finally, monitoring and early warning on drought related anomalies in vegetation development required observations at even higher spatial and temporal resolutions, while still covering large areas continuously.

INTRODUCTION

Climate variability has a very significant impact on the evolution of vegetation cover. This relationship can be analyzed using observations of climatic forcing factors and of vegetation response, using in both cases global data sets such as re-analysis data generated by means of atmospheric models and spectro-radiometric data collected by satellites. Available re-analysis data span a period of more than 40 years and the spectro-radiometric satellite data more than 25 years, sufficient to carry out studies of climatological relevance. Early examples of time series analysis of satellite data to study terrestrial vegetation and its response to climate variability were perfomed in the late 80s (Menenti *et al.*, 1991 and 1993).

The study of vegetation cover types, phenology and climate conditions by applying NOAAAVHRR NDVI imagery at regional scale has been successful (Townshend and Justice 1986, Justice *et al.* 1985, 1986). Potter and Brooks (1998) explained 70–80% of the spatial variability in the NDVI seasonal extremes for different plant functional types by means of climate indices involving temperature and rainfall. Henricksen and Durkin (1986) demonstrated that the start and the end of the growing season in Ethiopia, assessed with NDVI images, were strongly related to a moisture index. Also the integrals of NDVI for each growing season were found to be closely correlated with rainfall for the Sudanese savanna (Hielkema *et al.*, 1986). A strong linear relationship was found between NDVI and annual rainfall in the range of 150–1000 mm for the

western Sahel (Malo and Nicholson 1990). More recently, Anyamba and Tucker (2005) expanded the analysis of NDVI data on Sahelian vegetation dynamics as a proxy for the response of land surface to rainfall variabililiy for the period 1981–2003 and detected drought and 'wetter' conditions in agreement with the recent region-wide trends in rainfall. Justice *et al.* (1991) found a general relationship between rainfall estimates from Meteosat data and NOAA-AVHRR NDVI where the time lag between rains and NDVI was particularly noticeable where rainfall was the limiting factor for growth. Different authors demonstrated the usefulness of applying NOAAAVHRR NDVI to detect the effect of droughts in Ethiopia (Henricksen and Durkin 1986, Henricksen 1986) and in Sahel (Tucker *et al.,* 1986). Recently, NOAA-AVHRR NDVI series have been applied to study the interannual variability produced by ENSO events (Liu and Negrón Juárez 2001, Seiler and Kogan 2002, Gurgel and Ferreira 2003, Poveda and Salazar, 2004) to the point that Liu and Negrón Juárez (2001) could model high anomaly values of NDVI and ENSO indices to predict drought onset in Northeastern Brazil four months in advance with 68% success.

The novelty of our method is the simultaneous characterization of three aspects: spatial and temporal variability of vegetation cover and its dynamic response to forcing factors. This result is made possible by analysing time series for each image element (pixel). Analyses of the relationship between climate variability and photosynthetic activity were performed in Africa (Azzali and Menenti, 1999 and 2000), South America (Azzali and Menenti, 1999; Gonzalez-Loyarte and Menenti, 2008; Gonzalez-Loyarte *et al.*, 2008), Europe (Verhoef *et al.*, 1996; Roerink *et al.*, 2000) and China (Jia and Menenti, 2006). The impact of rainfall anomalies on vegetation phenology, in terms of timing (phase) and intensity of greenness, was studied by using Fourier series to fit a time series of NDVI observations. The study was performed in the northern semiarid region of Argentina where rainfall is the driving factor of vegetation phenology (Gonzalez-Loyarte and Menenti, 2008).

We have used this approach to study three different but related aspects:

- characterization and mapping of climate-soil-vegetation complexes (Menenti *et al.*, 1993; Azzali and Menenti, 1999 and 2000);
- quantitative analysis of the response of vegetation phenology to climate variability (Verhoef *et al.*, 1996; Roerink *et al.*, 2000; Gonzalez-Loyarte and Menenti, 2007);
- early detection of drought—related anomalies in vegetation phenology (Jia and Menenti, 2006).

Mapping Climate-Soil-Vegetation Complexes

The objective is to characterize and map areas wherein vegetation development is similar due to a unique combination of climate, soil and association of vegetation species. We have used the concise notation "isogrowth zones" to refer to these zones in our work. Isogrowth zones are mapped by applying classical numerical classification algorithms to maps of Fourier coefficients obtained by modeling the time series of NDVI observations for each pixel. The results of the classification are then analyzed and documented by correlation with soil maps and climate data. In all studies performed a clear correlation was observed between isogrowth zones and a measure of aridity such as the Budyko ratio.

Vegetation Phenology and Climate Variability

Climate forcing is accounted by using observations of net radiation and precipitation, more precisely their ratio (Budyko index), which is a measure of excess radiant energy at the land surface relative to available water and, therefore, of drought hazard. The response of vegetation as characterized by photosynthetic activity is obtained by estimates of the fraction of Absorbed Photosynthetically Active Radiation (fAPAR). These estimates are obtained with multispectral radiometric data collected by a family of imaging radiometers installed on satellites operated from 1979 onwards. The results summarized in this review were obtained with data collected by the' Advanced Very High Resolution Radiometer (AVHRR) and by the Moderate Resolution Imaging Spectroradiometer (MODIS).

Early Detection of Drought—Related Anomalies

The analysis of annual time series of NDVI observations shows (Jia and Menenti, 2006) that deviations of current year observations from the reference (average) year can be detected rather early in the growing season and that, once detected, provide useful information to predict the peak magnitude of anomalies well in advance of the actual occurrence of a drought spell. Modeling of NDVI time series by means of Fourier series or other techniques is used to fill gaps in the time series, including the ones due to clouds, to remove noise and to extrapolate in time using a moving window to compute the Fourier transform. The accuracy of the prediction increases with decreasing lead time, but the advance warning of an impending anomaly is by itself a useful information to deal with drought impacts, particularly on agriculture.

APPROACH

Fast Fourier Transform and Harmonic Analysis

The *Fast Fourier Transform* (FFT) algorithm used in this study allows to decompose the time profile of the NDVI series for each pixel, in an average signal plus N/2 sinusoidal components, with N being the length of the time series expressed as the number of images (Azzali and Menenti, 1996). The average signal is the mean NDVI value for the whole time series of observations and the periodic (sinusoidal) components are characterized by amplitude and phase. All of them, mean NDVI, and amplitude and phase for each period, are called in this paper Fourier parameters. Amplitude and phase are associated with a given period, e.g. 12 and 6 months in our analysis. The amplitude value represents a measurement of the maximum variability of NDVI at a given period, and phase is the timelag of this maximum in relation to the initial point of the series. The decomposition of a complex time series of NDVI images into simpler periodic signals allows to understand the relative weight of different periodic climate processes like rainfall and temperature on vegetation complexes (Azzali and Menenti, 2000) as well as foliar seasonality (Fuller and Prince 1996) in Southern Africa.

The *Harmonic Analysis* algorithm used in this study allows the use of irregularly spaced observations and the frequency of periodic functions can be selected by the user. The method has been described by Menenti *et al.* (1991, 1993 and 1995), Verhoef *et al.* (1996), Azzali and Menenti (1999 and 2000), Roerink *et al.* (2000 and 2003). This algorithm is a curve-fitting procedure based on harmonic components and it can be considered a generalisation of the maximum value compositing normally applied to generate NDVI data products. In practice time series of NDVI contain cloud—contaminated observations even after maximum value compositing The Harmonic Analysis of NDVI Time Series (HANTS) algorithm allows the user to select dominant frequencies, e.g. on the basis of a preliminary FFT analysis and applies a least squares fitting procedure based on the selected harmonic components. Filters can be defined to identfy and remove anomalous observations (Figure 1), due to e.g. clouds: this yields a time series of irregularly spaced observations, which may be different for each pixel. Although this flexibility comes at a price in terms of processing time, it does allow to maximize the number of valid observations and, therefore, of information extracted from the time series. Once the valid observations are fitted by the final Fourier series, the latter can be used to fill gaps in the observations for each final to obtain a cloud-free image of the area observed (Figure 2).

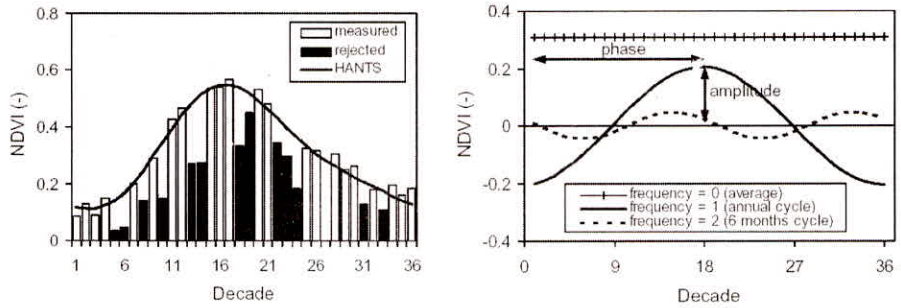

Fig. 1: Schematic description of the HANTS algorithm: (left) identification and removal of outliers and (right) resulting Fourier parameters of the filtered time series

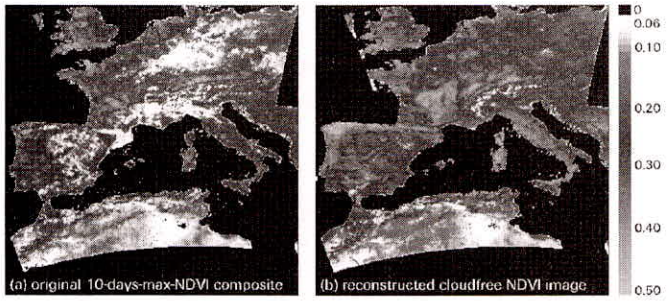

Fig. 2: Weekly composite NDVI image of Europe and North Africa: (left) original image with standard radiometric corrections and cloud flagging and (right) after removal of cloud contaminated observations and gap-filling using the HANTS algorithm

Large Area Mapping of Climate-Soil-Vegetation Complexes

Isogrowth-Zones

The most obvious feature of large area vegetation processes is the dynamics of land cover. Even without a precise definition of measurable parameters to characterize it, land cover dynamics is an integrated response to a variety of climate, biotic, physiographic and anthropic processes (Reichle, 1973; Lugo, 1974; Aber and Melillo, 1991; Swanson *et al.*, 1992; Walker, 1993; Turner *et al.*, 1994). It is this integrating function of land cover dynamics that provides a key to the description and understanding of large area ecosystems (Gosz, 1991; Johnson, 1990; Delcourt and Delcourt, 1992; Neilson 1986 and 1987). The use of temporal records of vegetation properties to characterize terrestrial ecosystems is a traditional research technique to understand the influence of weather and climate on vegetation (Leith, 1984; Reed *et al.*, 1994). Vegetation phenology is an extremely sensitive indicator of response to climate, soil and land management. The ability to study the timing of vegetation (green foliage) development and senescence with frequent and conistent observations is a powerful tool for the study of natural and agricultural environments. Examples of large-area phenological classification of vegetation using NOAA AVHRR NDVI data were given by Justice *et al.* (1985), Justice (1986), Lloyd (1990), Turcotte *et al.* (1993) and Running *et al.* (1994). The challenge was to develop an efficient approach to extract concise information from large amounts of data. Use of formal time series techniques provides a parsimonius description of phenology as shown by Menenti *et al.* (1991; 1993 and 1995), Eidenshink and Haas (1992), Eastman and Fulk (1993), Lambin and Strahler (1993), Viovy and Saint (1994) and Olsson and Ekhlund (1994).

Classification Algorithms

Both the FFT and the HANTS algorithms provide maps of Fourier coefficients, i.e. pixelwise values of amplitude and phase for all frequencies considered, thus providing maps of quantitative measurements of vegetation phenology. Such maps provide attributes of terrestrial vegetation that can be used to identify "isogrowth zones" in the sense explained above. To this end numerical classification procedures, such as generally used with spectral attributes of vegetation, can be applied. Contrary to classical numerical classification of spectral attributes at high spatial resolution, however, it is in general not feasible to define a-priori large area "isogrowth zones" and, therefore, classical supervised (hard) classification algorithms cannot be applied. Unsupervised and fuzzy classification techniques have in this context a significant potential. We have evaluated several alternate classification strategies and algorithms and two solutions have emerged:

(a) Apply first an unsupervised classification algorithm (see e.g. Tau and Gonzalez, 1974) to define classes and construct alternate sets of signatures; this is followed by the application of a supervised classification algorithm and using performance indicators (D'Urso and Menenti, 1996; Ayala and Menenti, 2002) to select the best definition of classes and associated signatures;

(b) Apply first an unsupervised classification algorithm, as above, followed by a fuzzy classification procedure; this strategy assigns membership values to each pixel for all classes considered, rather than assigning each pixel to a class only.

Both strategy (a) and (b) require an *ex-post* analysis on the basis of ancillary information such soil and vegetation maps to understand what each class actually means. The climate-soil-vegetation complexes or "isogrowth zones" can be then interpreted in terms of a combination of known attributes (Azzali and Menenti, 1996 and 2000).

Response of Vegetation Phenology to Climate Variability

Work done towards mapping the "isogrowth zones" documented a very close relationship between the results of vegetation mapping, done as described above, and aridity measured by using the Budyko ratio. These results document the correlation of spatial patterns. The next question is whether a similar relationship exists between temporal patterns or, in other words, whether the response of vegetation phenology, measured using time series of NDVI observations, can be related to climate forcing, measured by time series of the Budyko ratio.

The approach proposed is summarized by the diagram in Figure 3. To characterize vegetation phenology we have used the same data: time series of AVHRR and MODIS NDVI and fAPAR data products in a range of temporal and spatial resolutions. To obtain time series of maps of the Budyko ratio we have used re-analysis data generated by ECMWF and NCEP at a spatial resolution significantly lower than the spatial resolution of satellite data products. We assume that the latter describe the effect of spatial heterogeneity (soils, physiography and land management) within the larger grid cell for which re-analysis data are available.

The re-analysis data generated with atmospheric models have a spatial resolution (40 km ECMWF, 200 km NCEP) much lower than satellite data (1–4 km). Daily data on net radiation and precipitation have been

integrated over time to obtain data with the same temporal resolution as satellite NDVI and fAPAR data: from the 8 days of MODIS data to the 30 days of the AVHRR data used in our earlier studies. As mentioned the ratio of net radiation to precipitation is a measure of dryness and fAPAR (or NDVI) is a measure of photosynthetic activity. Given the significant difference in spatial resolution of the data on climate forcing respectively vegetation response, we have assumed that climate forcing is known and constant for a large area, while within it the spatial variability of vegetation response can be characterized using the higher resolution satellite data. In the earlier studies (Menenti *et al.*, 1993) the Normalized Difference Vegetation Index (NDVI) has been used as a surrogate of fAPAR. Vegetation response to dryness has been studied by using Fourier series to model the time series of the Budyko ratio respectively of fAPAR. This approach does also lead to identify the dominant periodic components in the observed signals.

Once the dominant frequencies have been identified, it becomes possible to study the phenological response of vegetation to drought, as measured by the time series of the Budyko ratio. This has been done by looking at both spatial and temporal correlation of Fourier coefficients, mainly the amplitudes of dominant components, with the yearly average of the Budyko ratio (Roerink *et al.*, 2003). The analysis has been also extended to interannual variability of phenology by evaluating the ratio of changes in Fourier coefficients to the corresponding changes in the Budyko ratio.

Early Detection of Anomalies in Vegetation Conditions

Very recently (Jia and Bastiaanssen, 2007) we went one step further: after studying stable spatial patterns of vegetation type and average aridity conditions and steady state yearly patterns of phenology and drought, we can now explore the use of time series analysis to model and predict observations and finally early detection of drought-related anomalies in vegetation phenology.

Vegetation response to drought can also be evaluated by analyzing the trends in time series of vegetation conditions observed by satellites. The trends in vegetation response can provide a measure of drought impact as well as a measure in drought evolution with time. These trends are fundamental for preparing short term predictions of biomass production and assess drought impact on crop yield and vitality of natural ecosystems.

For this purpose we have used data describing photosynthetic activity (e.g. the MODIS fraction of Absorbed Photosynthetic Active Radiation-fAPAR-data product, the Land Surface Temperature, vegetation indices, etc.) to provide a measure of the response of vegetation productivity (agriculture and forest) to drought.

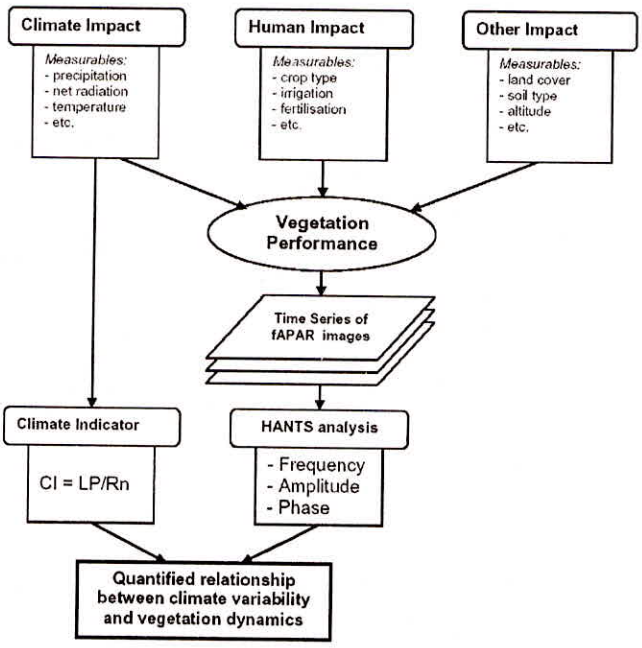

Fig. 3: Schematic description of the approach proposed in this paper to study the response of terrestrial vegetation to climate variability; CI is the ratio of precipitation times the latent heat of evaporation to net radiation

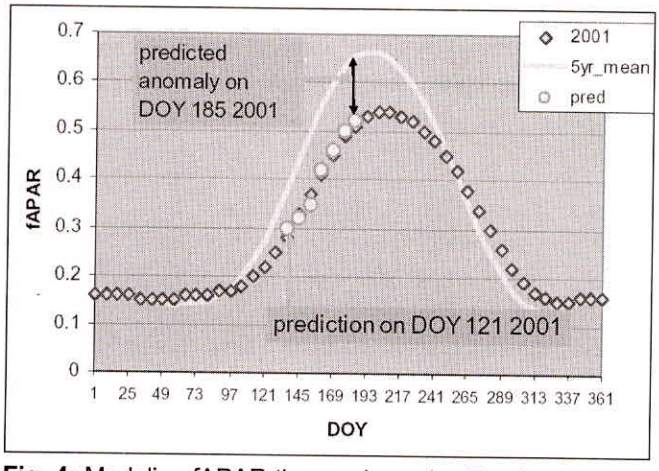

Fig. 4: Modeling fAPAR time series using Fourier analysis: observations for 2001 are modelled (squares) and compared with the average year for the period 1999–2006 (continuous line); on DOY 121 the modelled time series over the previous 12 months is used to predict the peak anomaly on DOY 185

The approach builds up on the concepts and methods described above. Given a multi-annual time series of observations, e.g. 8 days MODIS fAPAR, the Fourier

analysis is performed independently for each year. This gives a gap-filled, noise-filtered time series for each year in the data set and the average (reference) year. Occurrence and magnitude of drought-related anomalies, i.e. lower than average fAPAR and concurrent higher than average Budyko ratio, is evaluated first. Then modeling of a yearly time series is used to extrapolate in time the observations past the earliest observed anomaly, i.e. beyond the moment when the lower than average fAPAR is first detected (Figure 4).

Work on prediction of time series using a model determined on a moving segment of observations up to the date of prediction has just started and we expect to explore alternate methods (Fourier series, wavelets, Markov chains, etc) to model the time series of observations for each individual pixel. It should be noted that this approach yields maps of observed and predicted anomalies and of their magnitude.

METHODS

Fast Fourier Transform and Harmonic Analysis

For general information on Fourier series, Fourier transform and its applications in earth sciences the reader is referred to Fourier (1818), Box and Jenkins (1970), Brandt and Damen (1989) and Main (1990).

A time series of NDVI or fAPAR images will be indicated as $I(x, y, t)$, where x is pixel number or longitude, y is line number or latitude and t is time in dekades (10 days) or days. $I(x, y, t)$ can be expressed as a linear combination of elementary periodic functions,

$$I(x, y, t) = \sum_{n=1}^{L} A(x, y)_n \exp i[w_n t - g(x, y)_n \quad \ldots(1)$$

where w_n is frequency, A is amplitude and g is phase angle; the frequency is related to the period P_n as $w_n = 2\pi/P_n$. The maps $A(x, y)_n$ and $g(x, y)_n$ for the dominant terms in Eqn. (1) represent very concisely the information contained in the time series of image data $I(x, y, t)$.

The Fast Fourier Transform (FFT) algorithm.

A time series of equidistant data points of length N can be represented by a vector I of dimension N. The Fourier transform consists of finding the amplitude vector a, such that,

$$I = U a \quad \ldots (2)$$

Where U is a $N \times N$ matrix, which contains complex numbers u on the unit circle in the complex plane. Matrix U can be organized in such a way that each element $u_{r,k}$ is given by,

$$u_{r,k} = \exp\left[2\pi(r-1)(k-1)\frac{i}{N}\right] \quad \ldots (3)$$

Where r respectively k are the row respectively column number, and $i = \sqrt{-1}$. By multiplying the data vector I by the complex conjugate of U, U^* we obtain,

$$U^* I = U^* U a \quad \ldots (4)$$

and finally,

$$a = [U^* U]^{-1} U^* I \quad \ldots (5)$$

Since in the special case of the Fourier transform the matrix U is square and U^*U is diagonal and equal to NI, where I is the identity matrix, the solution in this case is simply,

$$a\left(\frac{1}{N}\right) U^* I \quad \ldots (6)$$

The mixed radix FFT algorithm implemented and applied for the investigations described in this Chapter is very fast because it calculates the matrix-vector product very efficiently by breaking it up in FFT-s of smaller dimensions. This is especially effective when N can be factored into many small (radix) numbers. In the present implementation of the algorithm the supported radix numbers are 2, 3, 4 and 5, which allows processing time series of such lengths (number of data points) as 12, 36 or 360. The latter allows the analysis of multi-annual data at e.g. dekadic temporal resolution.

A disadvantage of the FFT is that data points must be equidistant in time and that misisng data points are difficult to deal with. It would be desirable to weigh the input data to avoid missing data to have a large impact on the results. This has been implemented as detailed below.

The *Harmonic Analysis* algorithm.

To assign weights to the input data the Eqn. 2 must be rewritten as,

$$W I = W U a \quad \ldots (7)$$

Here the matrix U does not contain complex numbers anymore, but rather the associated sine- and cosine series. In this case multiplying by the transposed of U, U^* gives,

$$U^* W I = U^* W U a \quad \ldots (8)$$

with the solution,

$$a = [U^* W U]^{-1} U^* W I \quad \ldots (9)$$

where W is the diagonal matrix of weight factors. Because of these weight factors the matrix U^*WU is

not diagonal and its inverse must be determined in order to find the amplitudes.

This algorithm is the solution of a generic weighted least squares fitting problem and therefore it is applicable to a range of problems much wider than the FFT.

In the HANTS algorithm, as implemented, the matrix U has N rows and $2M + 1$ columns, where M is the number of frequencies to be considered above the zero frequency, except if $M = N/2$, in which case the number of columns is equal to N.

Large Area Mapping of Climate-Soil-Vegetation Complexes

Isogrowth—Zones

The areas wherein the phenology of terrestrial vegetation is similar were first identified then documented by going through the following steps:

(a) A multi-annual data set was prepared: we used ten years monthly NDVI data from August 1981 through July 1990 extracted from the archive created and maintained by the Global Inventory Monitoring and Modeling Systems team at NASA/GSFC. These are Global Area Coverage data reprojected to an equal area projection and re-sampled to obtain a 7.6 km × 7.6 km spatial resolution. These monthly composites are produced by first screening cloud-contaminated observations by using Thermal Infrared Radiance in the AVHRR Channel 5 and then searching for maximum NDVI within each month (Holben, 1986). This 10 years time series was constructed with radiometric data collected with three different AVHRR sensors and an intercalibration procedure was applied to remove sensor-related artifacts and trends (Los, 1993).

(b) The FFT mixed radix algorithm described above was applied to the time series of 108 monthly images. The images of mean NDVI and of the amplitudes of the 6 months, 1 year, 4.5 and 9 years components were retained for further analyses.

(c) The selected mean value and amplitude maps provide concise measurements of vegetation phenology and were used as attributes to identify homogeneous zones with the numeric classification procedures described below.

Classification Algorithms

Mapping of isogrowth zones (D'Urso and Menenti, 1996; Azzali and Menenti, 1996, 1999 and 2000) was done by going through the following steps:

(a) Most significant attributes were selected using a measure of separability (signature divergence);

(b) An unsupervised classification algorithm was used to construct alternate class definitions;

(c) Different alternate classification rules were applied;

(d) A measure of classification performance (IP) was constructed and used to compare the relatively large number of alternate classification procedures arisng from combinations of (a), (b) and (c). This indicator is based on normalized measures of reliability, separability and accuracy of classification.

(e) The highest value of IP leads to the best classification procedure.

The isogrowth zones, obtained by numeric unsupervised classification procedures, need to be documented on the basis of ancillary information on soils, climate and vegetation type. Climate was characterized using long term averages of net radiation and precipitation to construct maps of the mean Budyko ratio.

We have applied a fuzzy classification algorithm to gain some insights into a truly novel classification problem: classes could not be defined a-priori and maps of Fourier coefficients were to be used for the first time ever as class attributes. A fuzzy c-means (FCM) algorithm (Dunn, 1973; Bezdek *et al.*, 1984; Kent and Mardia, 1988) was coded and applied to explore how to best deal with this challenge. This method is a generalization of the hard c-means clustering algorithm: instead of assigning each pixel to a single class, it computes a measure of class membership for each pixel and for all classes. An initial set of classes is needed. The algorithm yields a map where each pixel is assigned to the class with the highest membership and one membership map for each class and all pixels.

The membership was evaluated as,

$$m_{ij} = \frac{d_{ij}^{-2(\varphi-1)}}{\sum_{j=1}^{M} d_{ij}^{-2(\varphi-1)}} \quad i = 1, ..., M;\ M < N \qquad \ldots (10)$$

where, m_{ij} = membership of pixel i for class j; d_{ij} = distance of pixel i from centroid of class j; φ = fuzziness exponent in the domain $(0, \infty)$; $\varphi = 1$ gives a hard classification, $\varphi = \infty$ gives uniform membership for all classes.

The objective of the tests with the FCM algorithm was to explore alternate ways to define classes. Cases where pixels have a large membership value for a single class and much lower values for the remaining classes suggest a feasible definition of classes. On the contrary, rather uniform membership values suggest that class definition is challenging.

Response of Vegetation Phenology to Climate Variability

The same data as described in Sect. 3.2 were used to characterize sensitivity of terrestrial vegetation to climate variability. The measurements of vegetation phenology provided by the Fourier coefficients were used to characterize vegetation response to climate characterized by the Budyko ratio. We have performed both a spatial and temporal analysis of the relation of vegetation phenology with aridity, as measured by the Budyko ratio.

The spatial analysis was done by correlating the maps of Fourier coefficients (mean value and amplitudes of dominant components) with the map of mean Budyko ratio.

The temporal analysis was done by computing ratios of interannual changes, such as,

$$\frac{\Delta A_n}{\Delta\left(\frac{R_n}{P}\right)} = \frac{A_n(\text{year}_l) - (\text{year}_k)}{\left(\frac{R_n}{P}\right)_{(\text{year}-l)} - \left(\frac{R_n}{P}\right)_{(\text{year}-k)}} \quad \ldots (11)$$

Where R_n is net radiation, P is precipitation, $year_l$ and $year_k$ are any paired years in the data set.

The correlation of spatial patterns of A_n and (R_n/P) for any given year k yields reationships of the kind,

$$A_n = f_k\left(\frac{R_n}{P}\right) \quad \ldots (12)$$

If this analysis is repeated for each annual data set, it is possible to evaluate the response of vegetation phenology to interannual variability of climate (dryness),

$$\frac{\partial A_n}{\partial t} = \frac{\partial f_k}{\partial\left(\frac{R_n}{P}\right)} \frac{\partial\left(\frac{R_n}{P}\right)}{\partial t} \quad \ldots (13)$$

where the temporal derivative is computed over any two years k and l. It should be noted that Equations 10 and 12 evaluate temporal response of vegetation phenology to interannual variability of dryness in two fundamentally different ways. Equation 12 assumes that the interannual variability of Fourier coefficients (amplitude in this case) can be computed as the product of the spatial dependence of A_n on (R_n/P) at constant t and the interannual change in (R_n/P). Equation 10 does not assume any spatial dependence of A_n on (R_n/P) and treats each pixel observation as independent.

We will evaluate whether Equations 10 and 12 lead to the same observed response of phenology to interannual variability in dryness by analysing extended time series of AVHRR data.

Early Detection of Anomalies in Vegetation Conditions

Time series analisis of NDVI and fAPAR image data has also been applied to detect drought-related anomalies. This requires modeling annual time series at weekly resolution or better, removing noisy and erroneous observations and filling resulting gaps.

The first step is to obtain a set of high quality annual time series, $I_k(x, y, t)$ and the time series for the average year, i.e. the time series of the mean value of $I_k(x, y, t)$ for all available observations on the same DOY over all available years,

$$\{I_1(x, y, t), ..., I_N(x, y, t)\} \Rightarrow \bar{I}(x, y, t) \quad \ldots (14)$$

Once this has been obtained, it becomes possible to define anomalies $D_k(x, y, t)$ as,

$$D_k(x, y, t) = [I_k(x, y, t) - \bar{I}(x, y, t)] \quad \ldots (15)$$

This procedure gives results as shown in Figure 4, which suggests that such smooth time series might be predictable by modeling a segment of the time series, from the date of the desired prediction backwards, and using the model to predict the time series forward.

RESULTS

The results reviewed here have been obtained in the context of several case studies (Table 1).

Table 1: Overview of Case-Studies on Fourier Analysis of Time Series of AVHRR—NDVI and MODIS fAPAR

Region	*Period*	*Spatial RES*	*Temporal RES*	*Method*	*Data*
Southern Africa	August 1981 – July 1990	7.6 km × 7.6 km	30 days	FFT	AVHRR—NDVI
South America	July 1982 – June 1991	7.6 km × 7.6 km	30 days	FFT, HANTS	AVHRR—NDVI
Argentina	January 1982 – June 1992	7.6 km × 7.6 km	30 days	HANTS	AVHRR—NDVI
Europe	January 1995 – December 1997	1 km × 1 km	10 days	HANTS	AVHRR—NDVI
China	January 2000 – December 2006	1 km × 1 km	8 days	HANTS	MODIS—APAR

Large Area Mapping of Climate-Soil-Vegetation Complexes

Southern Africa

A preliminary analysis of the significance of Fourier coefficients led to choose the mean NDVI, the amplitudes of the components with periods of 9, 4.5, 1 and 0.5 years and the phase of the of the components with periods of 1 and 0.5 years as most significant attributes of isogrowth zones.

The following elements were chosen to apply and evaluate alternate classification procedures to map the isogrowth zones:

- three sets of attributes;
- inclusion or exclusion by masking of ocean and inland water;
- normalization of numeric range of attributes;
- four different sets of signatures all including 20 classes, obtained by applying unsupervised classification;
- three different clustering rules for the supervised classification step.

Each combination of these elements yields a different classification procedure. For each procedure we evaluated the Reliability, Separability and Accuracy indicators and finally the overall classification performance indicator, IP. Out of all procedures, six had similar high IP values and were evaluated in more detail (Table 2).

A detailed, qualitative assessmefnt of procedures S2, S6, S7 and S12, all obtained using the maximum likelihood Bayesian decision rule, was performed by correlation with ancillary data. Although a comparably high performance was also obtained with procedure S1, we preferred to consider S2 in order to compare procedures based on the same decision rule.

The evaluation was done by overlaying each map of isogrowth zones with a map of the Budyko ratio, B, and the White (1983) map of the vegetation of Africa. At this stage all classes have been determined by numerical classification of the Fourier coefficients, so their significance needs to be understood and documented. A detailed analysis of these results was presented by Azzali and Menenti (1999 and 2000), here only a brief overview is given.

Isogrowth zones, as obtained with S2, correlate rather well with both the Budyko ratio (Figure 5a) and the White vegetation map (Figure 5b). The isoline of B = 2 for example describe rather well the transition zone between arid and semi-arid vegetation over a broad latitude range from the southern tip of Africa towards the sub-sahelian region. The agreement with the White vegetation map is also rather good, especially if we take into account that the White classes are broad association of species. Our isogrowth (or isophenology) map may define narrower vegation types. This is best documented by looking in some more detail at the features associated with each isogrowth zone.

Table 2: Reliability, Separability, Accuracy and Overall Performance Indicator, IP, for the Best Six Classification Procedures

Procedure	*Reliability*	*Separability*	*Accuracy*	*IP*
S1	0.71	1.40	0.85	0.885
S2	0.70	1.40	0.87	0.884
S6	0.65	1.395	0.92	0.884
S7	0.68	1.40	0.74	0.85
S9	0.70	1.405	0.48	0.79
S12	0.74	1.405	0.78	0.88

The maps in Figure 5 include 20 isogrowth zones: Azzali and Menenti described in detail the full legend of these map with a detailed analysis of the Fourier spectra, reconstructed NDVI(t) and the relative abundance of the White classes within each one of the 20 zones. Here we will give a few examples to document the correlation between increasing aridity (i.e. higher values of B), Fourier spectrum (amplitudes of different periodic components), the NDVI(t) reconstructed using the Fourier series and vegetation types as defined and mapped by White (1983).

Class 6 (and class 10) have the highest mean NDVI value in Southern Africa and Budyko values close to 1, thus showing a near equilibrium of evaporative demand (R_n) and water supply (P). Mean annual rainfall is 2000 mm. This class is located in the dense equatorial forest areas n Central Zaire, Congo and Gabon. According to White (1983) the vegetation is classified as wetter and drier Guineo-Congolian rain forest (Types 1a and 2, Figure 5b), swamp forest (type 8), mosaics of 1a and 8, mosaics of 1a, 2 and secondary grassland (11a). Class 6 (and class 10) is the only class having a dominant 6 months component and the reconstructed NDVI(t) shows a very well defined bimodal character.

Class 5 has a mean NDVI = 0.37 and B = 2. Mean annual rainfall varies overall between 800 mm and 1200 mm, while it is 500 mm in Kenya where B = 3. The vegetation consists of Somali–Masai Acacia—Commiphora deciduous bushland and thicket (White types 42, 16a and 11a). The NDVI(t) follows the rainfall pattern with a main peak in late fall. The 12 months component is dominant, although the 6 months component is still significant.

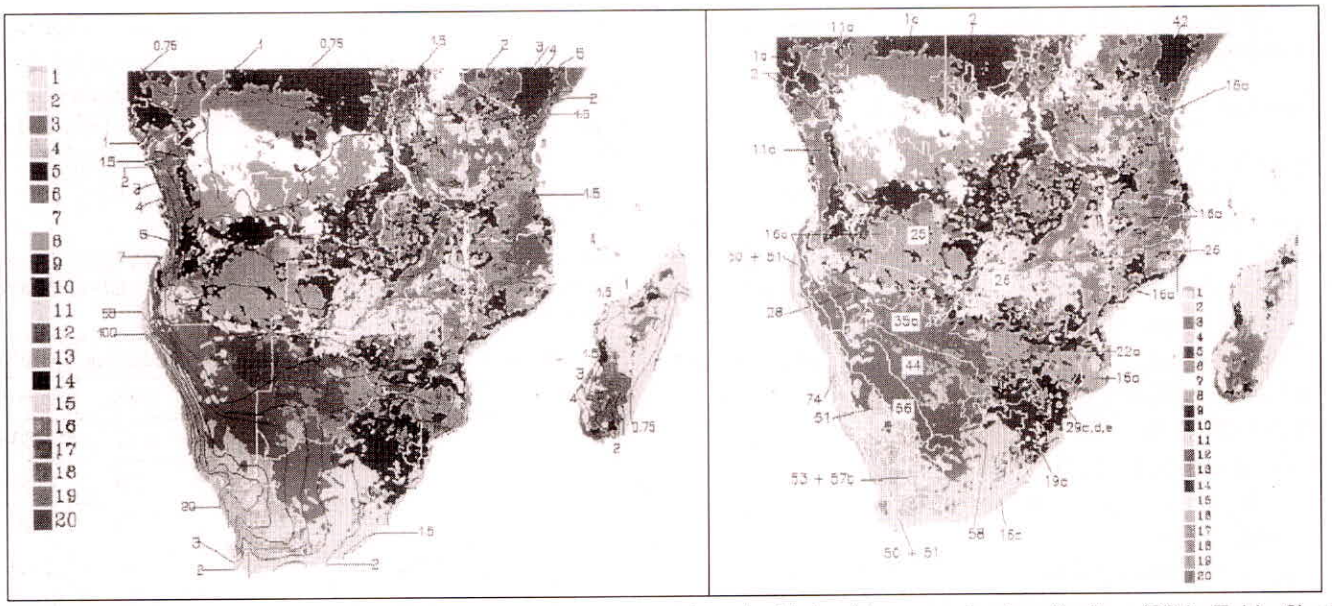

Fig. 5: Map of isogrowth zones (soil-climate-vegetation complexes) obtained by numeric classification (S2 in Table 2) of Fourier coefficients: a) overlain by isolines of the Budyko ratio and b) overlain by the White (1983) vegetation classes

Class 9 has a mean NDVI = 0.31 and B = 2.5. It is characterised by seasonal rainfall during the austral summer and a peak in January, with mean annual rainfall of 700 mm. The vegetation consists of high-yield grassland (type 58) and afromontane scrub forest (29c, d and e; 19a) according to White (1983). The sharp boundary between isogrowth zone 9 and zone 2 is most likely due to the higher fertility of soils within zone 9. The 12 months component is largely dominant and the amplitude is comparable with the mean NDVI. The significant amplitudes of the 9 and 4.5 years components suggest an influence of the middle Limpopo river on water supply to vegetation.

South America

The FCM method provides an alternate solution to the challenge of mapping vegetation at a spatial scale where it is not possible to define vegetation types precisely. As in the previous case-study on Southern Africa a subset of the Fourier coefficients obtained with the FFT were used as attributes to identify homogeneous zones. The NDVI(t) time series included the period 1982–1991 (see Table 1). The attributes were the mean NDVI, the amplitudes of the terms of the Fourier series with periods of 9, 4.5, 1 and 0.5 years and the phase values of the terms with periods of 1 and 0.5 years. Likewise the previous case, an unsupervised classification algorithm was used in a first step, but signatures were constructed for six classes only. Next, the membership of all pixels for the six classes was evaluated using Eqn. 10.

The FCM yields classification results as a set of maps: a first one where each pixel is assigned to the class for which membership is highest and M maps of the membership values of all pixels for each one of the M-classes. Part of this information can be merged into a single map (Figure 7), where colour indicates the class of highest membership and intensity its actual value.

The advantage of the FCM method is that it provides both broader map units and information on internal variability through the membership value. This is evident for example for the grasslands in south—eastern Argentina (Figure 7) where this broad vegetation type appears in magenta, with significant changes in intensity indicating subtler differences in the combination of species and vegetation conditions.

Response of Vegetation Phenology to Climate Variability

The relationship between vegetation type and aridity documented by the correlation of isogrowth zones with the Budyko ratio (see e.g. Figure 5) can be further analyzed by evaluation interannual variability of vegetation phenology and of climate. This relationship is confirmed by the dependence of both mean NDVI and the amplitude of the 1 year component on the value of B (Figure 8).

The values in Figure 8 were obtained by computing first the Fourier transform using HANTS for two yearly time series (1996 and 1997), then averaging the values of mean NDVI and amplitude obtained in each

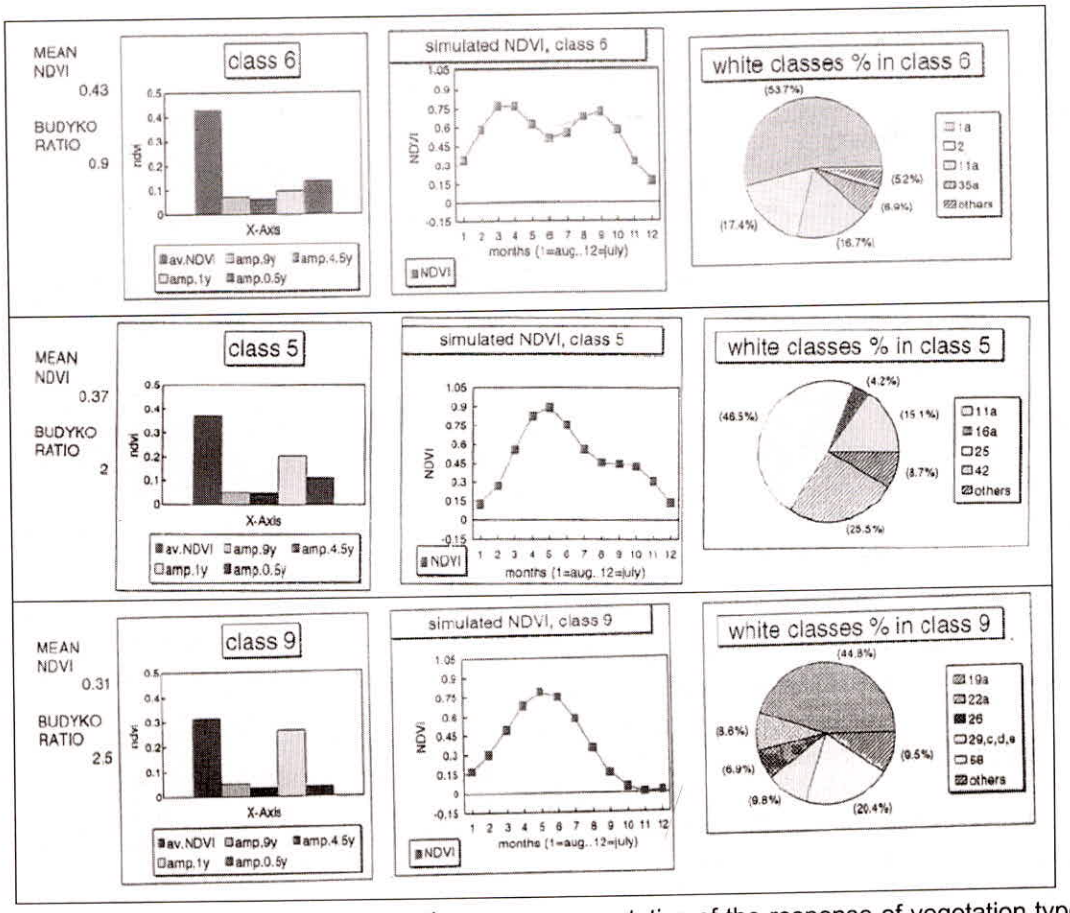

Fig. 6: Legend of the map in Figure 5 for isogrowth zones representative of the response of vegetation type to a broad range in aridity conditions; attributes of each isogrowth zone are: a) mean NDVI, b) mean B; c) Fourier spectrum; d) NDVI(t) reconstructed using the Fourier series and e) fractional abundance of White classes; classes 6, 5 and 9

Fig. 7: Map of isogrowth zones in South America showing classes 4, 5 and 6 of six fuzzy classes obtained with the FCM method (see text for details); colours indicate the class of highest membership and intensity indicates the membership value

year for all pixels and finally sampling the resulting maps to carry out the regression analysis. Scatter in data points clearly increases with decreasing number of pixels at increasing values of $(1/B)$. The latter indicator of climate conditions was used, instead of B, because of the wetter climate conditions in Europe compared with the previous case-studies in Southern Africa and South America.

The relationships in Figure 8 can be used to estimate the sensitivity, S, of vegetation phenology to water availability by computing,

$$S = \frac{\partial A_n}{\partial (P / R_n)} \qquad \ldots (16)$$

where $(1/B) = (P/R_n)$ is used instead of B taking into account the relatively wetter conditions of Europe.

This provides a straighforward measure of sensitivity to drought. Interesting is the difference in sensitivity between the mean NDVI and the 1 year amplitude. The value of S becomes negligible at $P/Rn \approx 1$ for mean NDVI and at $P/Rn \approx 1.5$ for the 1 year amplitude. Even more interesting is the difference between the value of S obtained using data over spatial patterns at given t, or data at different times for a given pixel, as in Eqn. 11.

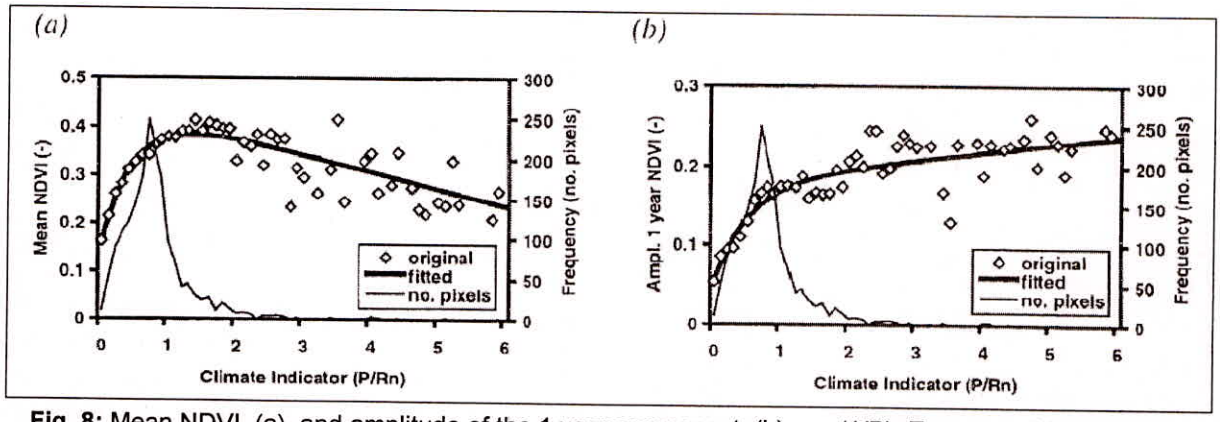

Fig. 8: Mean NDVI, (a), and amplitude of the 1 year component, (b), *vs.* (1/B); Europe and North Africa, AVHRR NDVI 1996–1997, 10 days composites at 1 km × 1 km resolution

A regression analysis on the data as in Figure 8 was performed to obtain the following relationship,

$$A_n = a + b\,(P/R_n) + cd^{\,p/Rn} \qquad \ldots (17)$$

Where the coefficients a, b, c and d depend on the order n of the periodic component under consideration. Since the Eqn. 17 has been obtained with data on spatial patterns at given t, this gives the dependence of vegetation phenology on spatial patterns in water availability. The sensitivity S can be computed using Eqn. 18, given Eqn. 17, obtaining a first derivative as a function of P/R_n.

We have used the Eqn. 11 to evaluate the sensitivity to temporal changes in water availability at a given location. It is rather evident that different functions $S(P/R_n)$ are obtained when either spatial patterns or interannual variability is considered (Figure 9).

Most interesting is the fact that S becomes negligible at significantly lower values of P/R_n in the case of interannual variability as compared with the case of spatial patterns: $P/R_n = 0.3$ for mean NDVI and $P/R_n \approx 0.8$ for the 1-year amplitude.

The value of S provides two different informations when computed in the time respectively space domain. In the time domain it provides a measure of the phenological response of vegetation established in an area with a given climate, i.e. a specific value of B, to a temporary and usually rather limited interannual change in B. We could, therefore, consider the value of S computed in the time domain, S_t, as a mesure of *resilience* of vegetation.

In the space domain, conversely, it provides a measure of differences in phenology of vegetation types established under different mean climate conditions, i.e. different mean B-values. This information may be interpreted as a measure of *vulnerability* of vegetation in the presence of long term changes in climate, i.e. such as to affect in a permanent way water availability at the locations considered to compute S in the space domain, S_s.

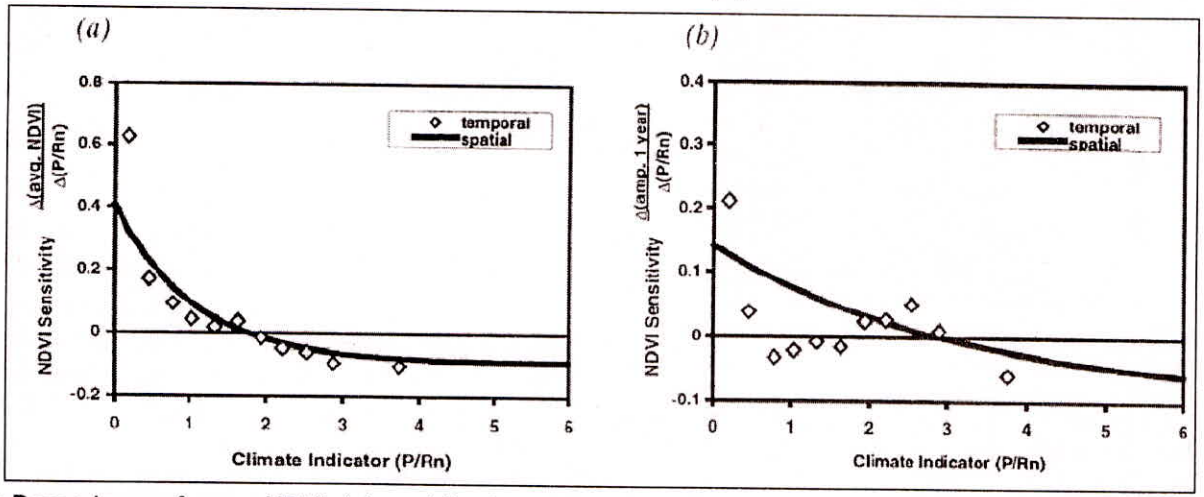

Fig. 9: Dependence of mean NDVI, (a), and the 1-year amplitude,(b), on water availability measured by the ratio P/R_n when considering spatial patterns (continuous line) and interannual variability (diamonds); Europe and North Africa, AVHRR NDVI 1995, 1996 and 1997, 10 days composites at 1 km × 1 km resolution

Early Detection of Anomalies in Vegetation Conditions

Timely and reliable detection of anomalies in vegetation conditions requires accurate removal of anomalous observations, filling gaps in the annual time series and robust modeling of the valid observations.

The result (see Eqn. 14) is a set of noise-free (or nearly so) annual time series and the time series for the reference year obtained all available observations for the same 8 days period. This provides a straight-forward way to determine (Eqn. 15) and visualize anomalies. A case-study (Jia and Menenti, 2006) on the Qinghai-Tibet Plateau using MODIS fAPAR data products for the period 2001–2005 illustrates how anomalies are detected and evaluated (Figure 10).

This illustrates the basic principle of the approach: although the overall shape of the fAPAR signature remains a simple periodic function, subtle differences in timing of minimum and maximum values and in the overall yearly amplitude are observable. Such differences are measured by using the Fourier parameters determined with HANTS.

Over vast and complex regions like the Qinghai-Tibet Plateau significant differences in interannual variability and phenology may occur and be observed. Anomalies may occur in some areas only, such as the case illustrated here. The driest (i.e. 2001) and the wettest (i.e. 2005) years were considered, but differences were almost negligible in the southeastern portion of the Plateau and very large, i.e. $\delta(R_n/\lambda P)$ = 13, in the northeastern Plateau where δfAPAR= –12. This example underscores the value of the approach described here: time series of spatial data on dryness conditions and concurrent vegetation conditions are essential to observe and understand the impact of climate variability on terrestrial vegetation. The latter is particularly relevant when observing extensive agricultural lands with the objective of monitoring and forecasting crop yields.

The latter has been the objective of a case-study on the severe 2006 drought in Sichuan and Chongqing, China.

This drought event was internationally widely reported. By 15 August 2006, natural disasters had killed 2,006 people, affected more than 316 10^6 others and caused economic losses of 160 10^9 yuan or 20 10^9 US$ (Jia and Bastiaanssen, 2007).

The analysis of MODIS fAPAR observations (Figure 11) shows that an anomaly was detected in the western part of the province as early as June 2nd 2006, which agrees with the rainfall anomaly detected with TRMM data in the same area and period of time. The improvement in spatial resolution obtained with the MODIS data, however, is very significant and of evident relevance to identify areas where drought remedial interventions are most needed. Moreover, while seasonal forecast of precipitation is a demanding challenge, the fAPAR anomaly develops as a smooth function of time (Figure 12), thus suggesting an easier prediction of trends and anomalies at different moments through the growing season.

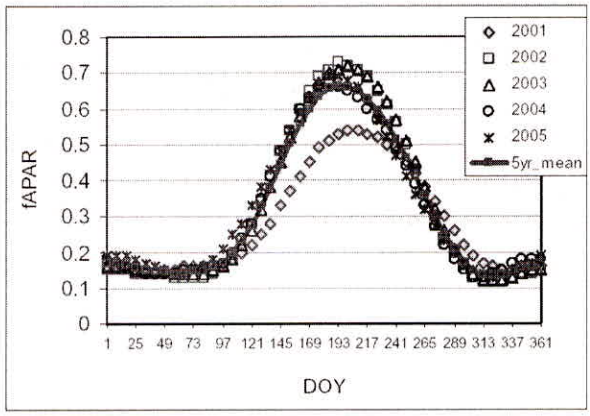

Fig. 10: Observed fAPAR annual time series at a randomly selected pixel in the Tibetan Plateau; each observation is a 8 days composite; Terra/MODIS, 2001–2205

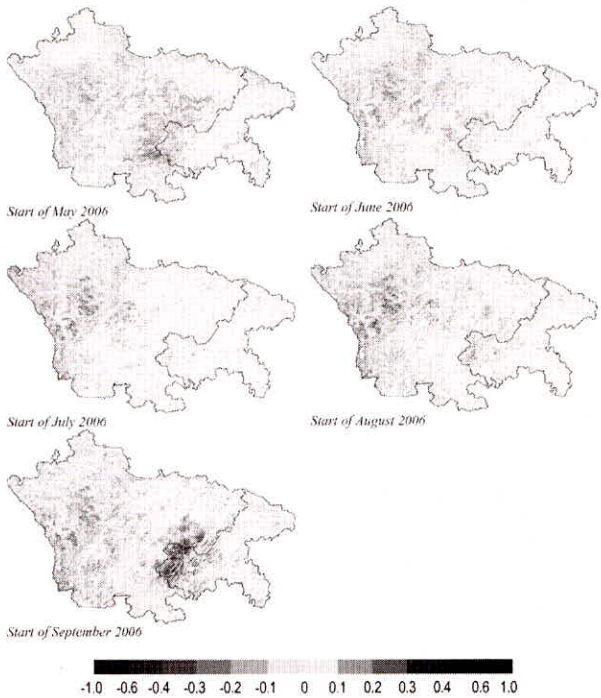

Fig. 11: Anomalies in the Fraction of Absorbed Photo-synthetically Active Radiation (fAPAR) observed by the MODIS satellite at 8 days intervals; anomaly is defined as difference between each 8 days value in 2006 and the corresponding average in the five year period 2001–2005; pixel size is 1 km × 1 km; Sichuan and Chongqing Provinces, China

The relevance of the method described here to drought early warning may become clearer by looking at temporal evolution of the anomaly for an individual pixel (Figure 12). Lower than average fAPAR values were observed as early as May 31st 2006 and this anomaly kept increasing until August 31st when recovery started. Although the anomaly was rather small in late spring, the smoothness of the signal and the memory of the process combine to yield a robust early warning information. The time series of maps of the anomaly (Figure 11) provides both the extent and severity of the event and might be used to identify areas requiring drought relief well in advance of reaching the peak severity of the anomaly. The maps indicate that an anomaly was first observed in early June in the central zone of Sichuan, but this anomaly receded during June and July. On the contrary the first signs of the more severe event in the zone across the border between Sichuan and Chongqing were observed in early August, while the anomaly peaked in early September.

Prediction of the anomaly by forward extrapolation of the time series is a possibility (see Figure 4), but work is in progress to evaluate alternate methods to model a segment of the time series from the point in time when the extraplotaion is required backwards, then using the model thus determined to extrapolate the time series forward.

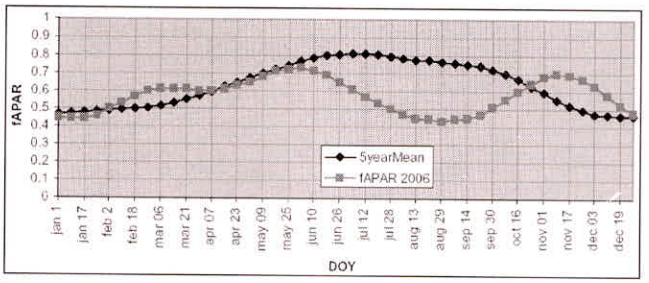

Fig. 12: Fraction of Absorbed Photosynthetically Active Radiation (fAPAR) observed by the MODIS satellite at 8 days intervals for a single pixel: five years(2001–2005) average (blue) and 8 days observations during 2006; pixel size is 1 km × 1 km; Sichuan Province, China

DISCUSSION

Large Area Mapping of Climate-Soil-Vegetation Complexes

The map of soil-climate-vegetation complexes (iso-growth zones) is a new type of map focussing on phytophenology and including for each class (complex) associations of different vegetation types. A straight-forward comparison of our map with vegetation maps such as the one by White (1983) and with the map of the Budyko *aridity index* map obviously shows some differences.

It should be noted that the main mapping units in the White map represent climax vegetation of different regions of endemism (White, 1983). The vegetation formations used in this context are usually rather broad, including large geographical locations and several lithological varieties, under climatic conditions that are also broadly defined.

The images of Fourier coefficients and associated statistics indicate that this new approach is very well suited to study phenology of terrestrial vegetation over large areas. Moreover the approach is useful in that temporal phenomena such as the seasonality of the vegetation can be displayed and understood in terms of 4 or 5 images instead of a large number, like the 108 AVHRR-NDVI images used in the Southern Africa and South America case-studies and the more than 250 MODIS-FAPAR images used in the China case study. Thus, the temporal behaviour vegetation communities manifested over many growing seasons may be summarized in a way that is potentially less cumber-some than other approaches (e.g. Malingreau, 1986).

The utility of the approach presented here to analyze multitemporal NDVI images may extend beyond mere description and summarization of foliar rythms observed at regional scale. For example, the 9-years amplitude image, which appears to relate to interannual variability of leaf display, may serve as a measure of resilience, an important functional response of vegetation to climatic change (Walker, 1991). In particular areas of high amplitude at low frequencies (i.e. those with periods of 9 and 4.5 years), such as *Acacia* woodland-bushland of the Kalahari, would suggest greater resilience to heightened climatic variation predicted for southern Africa under greenhouse warming scenarios (Pittock and Sallinger, 1991). Conversely, zones where the low frequency components showed small amplitudes, such as the miombo woodlands, would tend to indicate vegetation highly resistant to climatic changes. Of the two types of behaviour, it is likely that communities are able to adjust leaf display rapidly in response to changes in available resources (i.e. resilient forms) will be favoured under conditions of heightened climatic variations.

Response of Vegetation Phenology to Climate Variability

The results of the case-study carried out on Europe and North Africa presented here cover just three years, too short period of time to draw generic conclusions on the response of phenology to interannual climate variability. On the other hand a strong correlation has been found

between the Fourier coefficients and the ratio of precipitation over net radiation. The inverse of the Budyko ratio has been used in the study of Europe, because of the wetter conditions in comparsion with Southern Africa and South America. Among the amplitude and phase coefficients, the mean NDVI and the 1-year amplitude were the most sensitive indicators of vegetation response to climate variability.

The sensitivity of the Fourier amplitude and phase coefficients to climate variability was evaluated both in the time and spatial domain. In both cases the sensitivity decreased with increasing wetness (i.e. P/R_n). When considering changes in the spatial domain, the sensitivity S of mean NDVI becomes negligible at $P/R_n \approx 1.5$, while the S value for the 1-year amplitude becomes negligible at $P/R_n \approx 2.5$.

It is worth noting that negative S-values were obtained for the 1-year amplitude at $P/R_n \approx 0.5$, i.e. that the 1-year amplitude decreases with increasing wetness. This apparently contradictory result can be explained by considering that under semi-arid conditions, an increase in rainfall may increase minimum NDVI more than the maximum NDVI during the year, thus leading to smaller 1-year amplitudes.

Early Detection of Anomalies in Vegetation Conditions

The advance information on impending drought may be confirmed by concurrent observations of other land surface state variables, such as the Land Surface Temperature (LST). For the Sichuan and Chongqing case-study the LST anomaly anticipated the appearance of the fAPAR anomaly by a few weeks, but it was smaller throughout the period end of April 2006—end of August 2006. On the other hand, the LST anomaly once it appeared, it did not disappear, thus providing additional and useful information on the impending drought event, well in advance of the time of peak-severity (August 2006).

Moreover, both fAPAR and LST seem to respond consistently to climate forcing. An evaluation of fAPAR and LST response to rainfall, as estimated with TRMM data, was done by Jia and Bastiaanssen (2007). Although the very different spatial and temporal resolution of these rainfall (TRMM) and fAPAR (MODIS) observations does not allow a precise comparison, it is clear that the observed fAPAR anomaly responds rather well and correctly to the observed rainfall anomaly. The latter supports the use of fAPAR observations for detection and prediction of drought-related anomalies in the development of vegetation. Finally, it should be noted that in the Sichuan and Chongqing case-study anomalies and trends detected with diverse measures of water availability and of the response of terrestrial vegetation did add up to a coherent picture of the developing drought event about 2 months in advance of the time when anomalies reached their peak values in late August.

CONCLUSIONS

The 1-year and 6-months amplitudes, the 9-years amplitude and the 6-months phase images appear to relate to the distribution of vegetation types and thus these may be useful for developing image classifications based on temporal dynamics of the vegetation. Overall, aridity is a strong determinant of both vegetation type and of vegetation phenology. This was confirmed by a detailed correlation analysis of Fourier coefficients and Budyko index. The highest correlation coefficients were obtained for the 1-year and 6-months amplitude values. This information, combined with the agreement between the White (1983) vegetation map and our map of isogrowth zones, leads to the conclusion on the role of aridity, as measured by the Budyko ratio, in determining both phenology and vegetation type.

This conclusion is further strengthned by the fact that the map of isogrowth zones was obtained by a two-steps classification procedure: classes have been defined first by using an unsupervised classification algorithm to construct signatures in terms of Fourier coefficients, then the map proper has been produced. This implies that classes are entirely based on similarity of phenology as measured by the Fourier coefficients. Finally, the correlation of Fourier coefficients with B provides further evidence in support of the statements given earlier on the role of even small changes in aridity to determine subtle differences in vegetation types and, particularly, in the association of vegetation species.

The dependence of the NDVI Fourier spectra on climate variability in time and space has been established quantitatively. The correlation in the spatial domain was stonger than in the temporal domain, suggesting a measure of resilience of vegetation to interannual variability rather than adaptation to stable differences in dryness. Only under very dry conditions interannual variability has a larger impact on phenology than spatial variability in dryness.

The results on quasi-real-time monitoring and early warning of droughts are preliminary and much remains to be done on filtering and gap-filling of time series and, therefore, on the accurate and timely detection of

anomalies. The work presented here, however, shows that the information on vegetation phenology and photosynthetic activity conveyed by multi-spectral data collected by imaging radiometers is very reliable and relationships robust over a range of space and time scales.

The results summarized and reviewed in this chapter open up two main avenues for further research:

(a) The period of time spanned by spaceborne observations of the global land surface span, 25 years or more, having a climatological relevance far superior to what was achievable with the data available in the late '80-s when we began exploring these ideas; it deserves the most urgent attention, therefore, a deeper and more robust understanding of the observed response of the terrestrial biosphere to climate variability, specifically focusing on inter-annual variability.

(b) Both methods and data are now available to develop further an efficient and cost-effective early warning system on drought events, based directly on observations of vegetation conditions from space.

REFERENCES

Aber, J.D. and Melillo, J.M. (1991). *Terrestrial ecosystems.* Saunders College, Pub., p. 427.

Anyamba, A. and Tucker, C.J. (2005). "Analysis of Sahelian vegetation dynamics using NOAAAVHRR NDVI data from 1981–2003." *J. Arid Environments*, Vol. 63, 596–614.

Ayala, R.M. and Menenti, M. (2001). "Metodologia para la busqueda del major clasificador de imagenes de satellite." Teledeteccion, Medio Ambiente y Cambio Global, 469–472.

Azzali, S., and Menenti, M. (Eds) (1996). "Fourier Analysis of Temporal NDVI in the Southern African and American Continents Winand Staring Centre for Integrated Land, Soil and Water Research)." Wageningen, the Netherlands. *Report 108*, p. 151.

Azzali, S. and Menenti, M. (1999). "Mapping iso-growth zones on continental scale using temporal Fourier Analysis of AVHRR—NDVI data." *Int. J. Applied Earth Observation and Geoinformation,* Vol. 1 nr. 1: 9–20.

Azzali. S. and Menenti, M. (2000). "Mapping vegetation-soil-climate complexes in southern Africa using temporal Fourier analysis of NOAA—AVHRR NDVI data." *Int. J. Rem. Sens,* Vol. 21(5), 973–996.

Bezdek, J.C., Ehrlich, R. and Full, W. (1984). "FCM: the fuzzy c-means clustering algorithm." *Computer & Geosciences,* Vol. 10, 191–203.

Box, G.E.P. and Jenkins, G.M. (1970). "Time series analysis, forecasting and control. Holden Day", San Francisco, Ca., USA.

Brandt, S. and Damen, H.D. (1989). "Quantum mechanics on the personal computer." Springer Verlag, Heidelberg, Germany.

Budyko, M.I. (1958). "The Heat Balance of the Earth's Surface, trs. Nina A. Stepanova", US Department of Commerce, Washington, D.D., p. 259.

Budyko, M.I. (1974). "Climate and life." Academic Press, New York, p. 508.

Delcourt, P.A. and Delcourt, H.R. (1992). "Ecotone dynamics in space and time. In: A.J. Hansen and F. di Castri. Landscape boundaries." *Ecological Studies nr.* 92. Springer Verlag, New York, 19–53.

Dunn, J.C. (1973). "A fuzzy relative of the ISODATA process and its use in detecting compact, well separated clusters." *J. Cybern*, Vol. 3, 32–57.

D'Urso, G. and Menenti, M. (1996). "Performance indicators for the statistical evaluation of digital image classifications." *ISPRS Journal of Photogrammetry and Remote Sensing*, 51(2), 78–90.

Eastman, J.R. and Fulk, M. (1993). "Long sequence time series evaluation using standardized principal components." *Phot. Eng. & Remote Sensing,* Vol. 59(6), 991–996.

Eidenshink, J.C. and Haas, R.H. (1992). "Analyzing vegetation dynamics of land systems with satellite data." *Geocarto International*, Vol. 1, 53–61.

Fourier, J. (1818). "Note relative aux vibrations des surfaces élastiques et au mouvements des ondes." *Bulletin des Sciences par la Société Philomatique*, 126–136.

Fuller, D.O. and Prince, S.D. (1996). "Regional scale foliar phenology in tropical Southern Africa: an application of the Fast Fourier Transform to time series of satellite imagery." In: Azzali, S. and Menenti, M. (Eds). Fourier Analysis of Temporal NDVI in the Southern African and American Continents Winand Staring Centre for Integrated Land, Soil and Water Research. Wageningen, the Netherlands, *Report 108*: 114–134.

Gonzalez-Loyarte, M.M. and Menenti, M. (2008). "Impact of rainfall anomalies on Fourier parameters of NDVI time series of Northwestern Argentina." *Int. J. Rem. Sens*, Vol. 29(4), 1125–1152.

Gonzalez-Loyarte, M.M., Menenti, M. and Di Blasi, A.M. (2008). "Modelling bioclimate by means of Fourier analysis of NOAA-AVHRR NDVI time series in Western Argentina." *Int. J. Climatol.* DOI: 10.1002/ joc.1610.

Gosz, J.R. (1991). "Fundamental ecological characteristics of landscape boundaries." In: Holland, M.M. *et al.* (Eds.). Ecotones: the role of landscape boundaries in the management and restoration of changing environment. Chapman & Hall, London: 8–30.

Goward, S.N., Tucker, C.J. and Dye, D.G. (1985). "North American vegetation patterns observed with the NOAA-7 Advanced Very High Resolution Radiometer." *Vegetatio*, 64: 31–40.

Gurgel, H.C. and Ferreira, N.J. (2003). "Annual and interannual variability of NDVI in Brazil and its connections with climate." *Int. J. Rem. Sens*, Vol. 24, 3595–3609.

Henning, D. and Flohn, H. (1977). "Climate aridity index map." In: *Explanatory note of United Nations Conference on Desertification, 29 Aug. – 9 Sep. 1977, A/CONF* 74/31: 7–9.

Henricksen, B.L. (1986). "Reflections on drought: Ethiopia 1983–1984." *Int. J. Rem. Sens*, Vol. 7, 1447–1451.

Henricksen, B.L. and Durkin, J.W. (1986). "Growing period and drought early warning in Africa using satellite data." *Int. J. Rem. Sens*, Vol. 7, 1583–1608.

Hielkema, J.U., Prince, S.D. and Astle, W.L. (1986). "Rainfall and vegetation monitoring in the Savanna Zone of the Democratic Republic of Sudan using the NOAA Advanced Very High Resolution Radiometer." *Int. J. Rem. Sens*, Vol. 7, 1499–1513.

Jia, L. and Menenti, M. (2006). "Response of vegetation photosynthetic activity to net radiation and rainfall: a case study on the Tibetan Plateau by means of Fourier analysis of MODIS fAPAR time series." *Advances in Earth Sciences*, 21(21): 1254–1259.

Jia, L. and Bastiaanssen, W.G.M. (2007). "Cost-Benefit Analysis: China Drought Monitoring and Prediction Tool. A brief case study of the 2006 Sichuan Drought." *Report of Preparatory Study*. Alterra, Wageningen University and Rsearch Centre, p. 31.

Johnson, L.B. (1990). "Analyzing spatial and temporal phenomena using GIS—A review of ecological applications." *Landscape ecology*, Vol. 4(1), 31–43.

Justice, C.O., Townshend, J.R.G., Holben, B.N. and Tucker, C.J. (1985). "Analysis of the phenology of global vegetation using meteorological satellite data." *Int. J. Rem. Sens*, Vol. 6, 1271–1318.

Justice, C.O. (Ed.) (1986). "Monitoring the grasslands of semi-arid Africa using NOAA-AVHRR data." *Int.J. Rem. Sens.* Vol. 7 (11) Special Issue, 1383–1622.

Justice, C.O. and Hiernaux, P.H.Y. (1986). "Monitoring the grasslands of the Sahel using NOAA AVHRR data: Niger 1983." *Int.J. Rem. Sens*, Vol. 7: 1475–1497.

Justice, C.O., Dugdale, G., Townshend, J.R.G., Narracott, A.S. and Kumar, M. (1991). "Synergism between NOAA-AVHRR and Meteosat data for studying vegetation development in semi-arid West Africa." *Int.J. Remote Sensing*, Vol. 12, 1349–1368.

Kent, J.T. and Mardia, K.V. (1988). "Spatial classification using fuzzy memberships models." *IEEE Trans.* On PAMI, Vol. 10(5), 659–671.

Lambin, E.F. and Strahler, A.H. (1993). "Change-vector analysis in multitemporal space: a tool to detect and categorize land-cover change processes using high temporal resolution satellite data." *Rem. Sens. Environ*, Vol. 48, 231–244.

Leith, H. (Ed.) (1974). "Phenology and seasonality modeling." Springer, New York.

Liu, W.T. and Negrón Juárez, R.I. (2001). ENSO drought onset prediction in northeast Brazil using NDVI. *Int.J. Rem. Sens,* Vol. 22, 3483–3501.

Lloyd, D. (1990). "A phenological classification of terrestrial vegetation cover using shortwave vegetation index imagery." *Int. J. Rem. Sens,* Vol. 12, 2269–2279.

Lugo, A. (1974). "Tropical ecosystem structure and function." In: Farnworth, E.G. and Golley, F.B. (Eds.. *Fragile ecosystems*. Springer Verlag, New York, 67–111.

Main, I.G. (1990). *Vibrations and Waves in Physics*. Cambridge Univ. Press, p. 356.

Malo, A.R. and Nicholson, S.E. (1990). "A study of rainfall and vegetation dynamics in the African Sahel using normalized difference vegetation index." *J. Arid Environments,* Vol. 19, 1–24.

Menenti, M., Bastiaanssen, W.G.M., Hefny, K. and Abd El Karim, M.H. (1991). "Mapping of groundwater losses by evaporation in the Western Desert of Egypt." *Report 43*. DLO Winand Staring Centre, Wageningen, The Netherlands, p. 116.

Menenti, M., Azzali, S., Verhoef, W. and van Swol, R. (1993). "Mapping agroecological zones and time lag in vegetation growth by means of Fourier analysis of time series of NDVI images." *Adv. Space Res*, 13(5): 233 237.

Menenti, M., Azzali, S. and Verhoef, W. (1995). "Fourier analysis of time series of NOAA-AVHHR NDVI composites to map isogrowth zones." In: Zwerver, S. *et al.* (eds.), *Climate change research: evaluation and policy implications*. Elsevier, Amsterdam, 425–430.

Myneni, R.B., Knyazikhin, Y., Zhang, Y., Tian, Y., Wang, Y., Lotsch, A., Privette, J.L., Morisette, J.T., Running, S.W., Nemani, R., Glassy, J. and Votava, P. (1999). "MODIS leaf area index (LAI) and fraction of photosynthetically acng tive radiation absorbed by vegetation (FPAR) product (MOD15) Algorithm Theoretical Basis Document, Version 4.0."

Neilson, R.P. (1986). "High resolution climatic analysis and southwest biogeography." *Science*, Vol. 232, 27–34.

Neilson, R.P. (1987). "Biotic regionalization and climatic controls in Western North America." *Vegetatio*, Vol. 70, 135–147.

Olsson, L. and Eklundh, L. (1994). "Fourier series for analysis of temporal sequences of satellite sensor imagery. *Int. J. Rem. Sens,* Vol. 5(18), 3735–3741.

Potter, C.S. and Brooks, V. (1998). "Global analysis of empirical relations between annual climate and seasonality of NDVI." *Int. J. Rem. Sens,* Vol. 19, 2921–2948.

Poveda, G. and Salazar, L.F. (2004). "Annual and interannual (ENSO) variability of spatial scaling properties of a vegetation index (NDVI) in Amazonia." *Rem. Sens. Environ*, Vol. 93, 391–401.

Reed, B.C., Brown, J.F., Vanderzee, D., Loveland, T.R., Merchant, J.W. and Ohlen, D.O. (1994). "Measuring phenological variability from satellite imagery." *J. Vegetation Science*, Vol. 5, 703–714.

Reichle, D.E. (Ed.) (1973). "Analysis of temperate forest ecosystems." *Ecological Studies 1.* Springer Verlag, New York.

Richards, Y. and Poccard, I. (1998). "A statistical study of NDVI sensitivity to seasonal and interannual rainfall variations in Southern Africa." *Int. J. Rem. Sens*, Vol. 19, 2907–2920.

Roerink, G.J., Menenti, M. and Su, Z. (1999). "A method for assessment of interannual climate variability by using Fourier components." *Proceedings International Geoscience and Remote Sensing Symposium* (IGARSS), Hamburg, IGARSS'99: 681–693.

Roerink, G.J., Menenti, M. and Verhoef, W. (2000). "Reconstructing cloud-free NDVI composites using Fourier analysis of time series." *Int. J. Rem. Sens*, Vol. 21(9), 1911–1917.

Roerink, G.J., Menenti, M., Soepboer, W. and Su, Z. (2003). "Assessment of climate impact on vegetation dynamics by using remote sensing." *Phys. Chem. Earth*, Vol. 28: 103–109.

Running, S.W., T.R. and Pierce, L.L. (1994). "A vegetation classification logic based on remote sensing for use in global biogeochemical models." *Ambio,* Vol. 23(1): 77–81.

Seiler, R.A. and Kogan, F. (2002). "Monitoring ENSO cycles and their impacts on crops in Argentina from NOAA-AVHRR satellite data." *Adv. Space Res*, Vol. 30, 2489–2493.

Spanner, M.A., Pierce, L.L., Running, S.W. and Peterson, D.L. (1990). "The seasonality of AVHRR data of temperate coniferous forests: relationship with leaf area index." *Rem. Sens. Environ*, Vol. 33: 97–112.

Swanson, F.J., Wondzell, S.M. and Grant, G.E. (1992). Landforms, disturbance ecotones. In: Hansen, A.J. and di Castri, F. "Landscape boundaries." *Ecological Studies nr. 92*. Springer Verlag, New York, 304–323.

Tau, J.T. and Gonzalez, R.C. (1974). "Pattern recognition principles." *Applied mathematics and computation nr. 7.* Addison Wesley, p. 377.

Townshend, J.R.G. and Justice, C.O. (1986). "Analysis of the dynamics of African vegetation using the normalized difference vegetation index." *Int. J. Rem. Sens*, Vol. 7, 1435–1445.

Tucker, C.J., Justice, C.O. and Prince, S.D. (1986). "Monitoring the grasslands of the Sahel 1984–1985." Int. J. Rem. Sens, Vol. 7, 1571–1581.

Turcotte, K.M., Lulla, K. and Venugopal, G. (1993). "Mapping small scale vegetation changes of Mexico." *Geocarto International,* Vol. 4: 73–85.

Turner, B.L., Meyer, W.B. and Skole, D.L. (1994). "Global land use/land cover change: towards an integrated study." *Ambio*, Vol. 23(1), 91–95.

Verhoef, W., Menenti, M. and Azzali, S. (1996). "A colour composite of NOAA-AVHRR-NDVI based on time series analysis 1981-1992." *Int. J. Rem. Sens*, Vol. 17: 231–235.

Viovy, N. and Saint, G. (1994). "Hidden Markov models applied to vegetation dynamics analysis using satellite remote sensing." *IEEE Trans.* Geosc. & Rem. Sens, Vol. 32(4), 906–917.

Walker, B.H. (1993). "Rangeland ecology: understanding and managing change." *Ambio*, Vol. 22(2–3): 80–87.

White, F. (1983). "The vegetation of Africa: a descriptive memoir to accompany the UNESCO/AETFAT/UNSO vegetation map of Africa." *Natural Resources Research*, Vol. 20, UNESCO, Paris, p. 356.